Scalar time domain modeling and coupling of second harmonic generation process in GaAs discontinuous optical waveguide

A. Massaro, V. Tasco, M. T. Todaro, R. Cingolani, M. De Vittorio, and A. Passaseo

National Nanotechnology Laboratory of CNR-INFM , Distretto Tecnologico-ISUFI, Università del Salento, Via Arnesano 16, 73100 Lecce, Italy.
alessandro.massaro@unile.it

Abstract: We present in this work the scalar potential formulation of second harmonic generation process in $\chi^{(2)}$ nonlinear analysis. This approach is intrinsically well suited to the applications of the concept of circuit analysis and synthesis to nonlinear optical problems, and represents a novel alternative method in the analysis of nonlinear optical waveguide, by providing a good convergent numerical solution. The time domain modeling is applied to nonlinear GaAs asymmetrical waveguide with dielectric discontinuities in the hypothesis of quasi phase matching condition in order to evaluate the efficiency conversion of the second harmonic signal. The accuracy of the modeling is validated by the good agreement with the published experimental results. The effective dielectric constant method allows to extend the analysis also to 3D optical waveguides.

OCIS codes: (000.4430) Numerical approximation and analysis; (310.0310) Thin films.

References and links

1. T. Rozzi and M. Farina, *Advanced electromagnetic analysis of passive and active planar structures*, (IEE Electromagnetic wave series 46, London. 1999), ch.2.
2. C. G. Someda, *Onde elettromagnetiche*, (UTET Ed., Torino. 1996), ch. I.
3. M. A. Alsunaidi, H. M. Masoudi, and J. M. Arnold, "A time-domain for the analysis of second harmonic generation in nonlinear optical structures," IEEE Photon. Technol. Lett. **12**, 395–397 (2000).
4. A. Massaro and T. Rozzi, "Rigorous time-domain analysis of dielectric optical waveguides using Hertzian potentials formulation," Opt. Express **14**, 2027-2036 (2006).
5. A. Massaro, M. Grande, R. Cingolani, A. Passaseo, and M. De Vittorio, "Design and modeling of tapered waveguide for photonic crystal slab by using time-domain Hertzian potentials formulation," Opt. Express **15**, 16484-16489 (2007).
6. N. Marcuvitz, and J. Schwinger, "On the representation of the electric and magnetic field produced by currents and discontinuities in wave guides," J. Appl. Phys. **22**, 806-820 (1951).
7. N. C. Frateschi, A. Rubens, and B. De Castro, " Perturbation theory for the wave equation and the effective refractive index approach," IEEE J. Quantum Electron. **QE-22**, 12-15 (1986).
8. A. Yariv, *Quantum Electronics*, (John Wiley & Sons , 3rd ed., Canada.1989), ch. 22.
9. L. Striscione, M. Centini, C. Sibilia, and M. Bertolotti, "Entangled guided photon generation in (1+1)-dimensional photonic crystals," Phys. Rev. A **74**, (2006).
10. A. Taflove and S. C. Hagness, *Computational Electrodynamic: the Finite-difference Time-domain Method*, (Arthec House Publishers, sec. ed., London 2000), ch. 2,3,4,7.
11. G. Mur, "Absorbing boundary conditions for the finite-difference approximation of the time-domain electromagnetic field equations," IEEE Trans. Electromagn. Compat. **23**, 377-382 (1981).
12. G. Khanarian, "Theory of design parameters for quasi-phase-matched waveguides and application to frequency doubling in polymer waveguides," IEEE J. Select. Topics in Quantum Electron. **7**, 793-805 (2001).
13. E. U. Rafailov, P. L. Alvarez, C. T. A. Brown, W. Sibbett, R. M. De la Rue, P. Millar , D. A. Yanson, J. S. Roberts, and P. A. Houston, "Second-harmonic generation from a first-order quasi-phase-matched GaAs/AlGaAs waveguide crystal," Opt. Lett. **26**, No. 24, 1984-1986 (2001).

#97297 - $15.00 USD Received 10 Jun 2008; revised 22 Jul 2008; accepted 1 Aug 2008; published 2 Sep 2008

14. A. Massaro, L. Pierantoni, and T. Rozzi, "Accurate analysis and modelling of laminated multilayered 3-D optical waveguides," IEEE J. Quantum Electron. **40**, 1478-1489 (2004).
15. T. Suhara, and H. Nishihara, "Theoretical analysis of waveguide second-harmonic generation phase matched with uniform and chirped grating," IEEE J. Quantum Electron. **26**, 1265-1276 (1990).
16. A. Yariv, "Coupled-mode theory for guided-wave optics," IEEE J. Quantum Electron. **9**, 919-933 (1973).

1. Introduction

With the introduction of rigorous time domain methods with analytical approximations it is possible to represents the physical phenomena such as light propagation and second harmonic generation (SHG) process inside a nonlinear optical device with a good convergent solution and low computational cost. For this reason a time domain simulator containing second-order nonlinearities, and including numerical approximations of dielectric step discontinuities, is presented in this work. The simulation algorithm is based on nonlinear wave equations associated to the circuital approach which considers the time-domain wave propagating in nonlinear transmission lines. The transmission lines represent the propagating modes of a non linear optical waveguide. Each propagating mode is solution of the scalar Helmholtz wave equation [1]-[5] and is associated to a transmission line with a characteristic impedance which depends on the modal effective refractive index. This analogy allows to model a nonlinear optical waveguide as a set of transmission line circuits which take into account the dielectric interfaces along the propagating direction as voltage and current generators. In the frequency domain, the transmission and reflection properties of dielectric discontinuities may be derived by means of an equivalent circuit [6],[7],[8] that automatically ensures continuity of the fields and their first derivatives along the propagation-directions. If potentials are used, instead, second derivatives are involved and generators are necessary at each dielectric interface in order to model accurately the discontinuous regions of the periodic nonlinear waveguide. These generators allow to model a discontinuous optical waveguide by decreasing the computational cost with good convergent solution [5]: the generators are placed directly on the interface nodes by optimizing the numerical error of the temporal second derivates at the dielectric boundary condition. In this way it is also possible to discretise complex nonlinear dielectric thin multilayer structure with cells size of the same order of the dielectric thicknesses, by obtaining a convergent solution [5]. By using this approach the SHG process is treated as a simple equivalent scalar problem with a numerical accuracy provided by the generators.

For a two-dimensional (2-D) SHG problem the proposed time-domain algorithm solves rigorously harmonic field by considering only two coupled equations between a fundamental nonlinear equation and a second harmonic (SH) nonlinear equation. For the same problem, the conventional finite difference time domain (FDTD) algorithm solves for three field components which are correlated, by increasing of 50% the central processing unit (CPU) time. In a 3D case the proposed algorithm solves again two scalar equations instead of six, and subsequently all the electromagnetic (EM) field components are obtained by the two scalar potentials as in Hertzian potential formulation (HPF) [4],[5]. By considering the numerical approximation (voltage and current generators of Fig. 1) with the analytical approximation (effective dielectric constant (EDC) method) we model in this work GaAs nonlinear discontinuous waveguides for wavelength conversion applications. Wavelength conversions of lasers are fundamental techniques in optoelectronics. These techniques require the phase coincidence of optical waves generated in nonlinear medium to obtain high conversion efficiency. Among various kind of phase matching device, quasiphase matching (QPM) is a most promising method because QPM can use the maximum nonlinear optical tensor component with flexibility of designed phase matching wavelength. The QPM application in high efficiency SHG processes is analyzed in this work in which we model the $\chi^{(2)}$ non linear process in the asymmetrical GaAs slab waveguide with nonlinear core and dielectric discontinuities: in the nonlinear planar waveguides a fundamental mode can couple to a second-harmonic SH mode through an appropriate nonlinear susceptibility coefficient. The circuital model is applied to GaAs discontinuous slab waveguide at different working

#97297 - $15.00 USD Received 10 Jun 2008; revised 22 Jul 2008; accepted 1 Aug 2008; published 2 Sep 2008

wavelengths in order to estimate the SH conversion efficiency in QPM condition. A good agreement between experimental results (reported in [13]) and numerical results confirms the rigorous accuracy of the proposed time domain circuital approach. The EDC method is used in the time domain modeling in order to analyze a 2D problem in a 1D case. The same EDC approach and the coupling mode theory extend the analysis for a 3D GaAs discontinuous ridge waveguide in QPM condition, by providing also the optimum grating lengths for a high SH conversion efficiency: the coupling coefficient along the propagating direction allows to design the total grating length in order to obtain a good SH enhancement at the end of the periodic structure. In particular we analyze the 3D ridge waveguide commonly used in demultiplexing and optical filtering applications.

We summarize the presented work in the following steps: i) we first test the new time domain modeling including generators with the experimental results of a nonlinear GaAs waveguide at working wavelength (wavelength of the fundamental mode) λ=1.955 μm; ii) we apply the numerical method to discontinuous nonlinear GaAs waveguide for telecommunication applications at λ=1.55 μm by evaluating the SH efficiency conversion in QPM condition; iii) we use the QPM condition and the coupling mode theory in order to evaluate the total grating length of a practical 3D ridge waveguide with nonlinear GaAs core on AlGaAs substrate at the working wavelength of λ=1.55 μm. The grating length design is analyzed by considering the coupled mode theory with the assumption of linear material in order to define the grating length related to a good coupling between the fundamental and SH mode, considered as ideal modes without losses in phase matching condition. The steps listed above are reported in details in the block diagram of Fig. 2.

2. Second harmonic generation process: scalar time domain modeling of discontinuous waveguides.

The formulation of the fundamental and second-harmonic fields starts with the Helmholtz wave equation for an homogeneous non-dissipative medium:

$$\nabla^2 \Psi_{e,h}(x,y,z,t) - \mu\varepsilon_{eff} \frac{\partial^2 \Psi_{e,h}(x,y,z,t)}{\partial t^2} = 0 \tag{1}$$

where ψ_e and ψ_h represent two guided modes of the asymmetrical waveguide shown in Fig.1 (a), and ε_{eff} is the effective permittivity index evaluated by the EDC method [7]. Each mode propagates in the optical waveguide as a signal which travels in a transmission line (see Fig. 1 (b)) characterized by a characteristic impedance given by

$$Z_{e,h} = \frac{1}{\sqrt{\varepsilon_{eff_{e,h}}}} \sqrt{\frac{\mu_0}{\varepsilon_0}} \tag{2}$$

It is known that the scalar wave equation may lead to inconsistencies because, in inhomogeneous regions such as step discontinuities shown in Fig.1 (a), it is, in general, not equivalent to Maxwell's equations. Electromagnetic scattering problems, including free space, involve the calculation of the fields produced in the presence of geometrical discontinuities by arbitrary currents and voltages [4]. Such discontinuities may be replaced by equivalent generators [4],[5], (see Fig. 1 (b)), giving an accurate solution of the EM field for structures with high dielectric contrast. In fact the scalar wave equation Eq. (1) for a non-dissipative medium can be rewritten as

$$\nabla^2 \Psi_{e,h}(x,y,z,t) - \mu\varepsilon_{eff} \frac{\partial^2 \Psi_{e,h}(x,y,z,t)}{\partial t^2} - \mu \frac{\partial^2 P^{e,h}_{pert}(x,y,z,t)}{\partial t^2} = 0 \tag{3}$$

#97297 - $15.00 USD Received 10 Jun 2008; revised 22 Jul 2008; accepted 1 Aug 2008; published 2 Sep 2008

where

$$P^{e,h}{}_{pert}(\mathrm{x,y,z,t}) = \Delta\varepsilon(x,y,z,t)\Psi_{\mathrm{e,h}}(x,y,z,\mathrm{t}) \tag{4}$$

represents the dielectric polarization and in a 1D case [4]

$$\Delta\varepsilon = \varepsilon_{i+1} - \varepsilon_i \quad i = z \text{ longitudinal position} \tag{5}$$

Equation (3) gives the effect of the generators $V_{f,s}$ and $I_{f,s}$ reported in Fig.1 (b) as variation of coefficients in the finite difference (FD) field discretisation [4]. In particular the wave solution in the homogeneous region (uniform slab region without discontinuities) is in the iterative form [4]

$$\Psi^{n+1}_{e,h}(i) = \Psi^{n}_{e,h}(i+1)\left(\frac{b}{a}\right) + \Psi^{n}_{e,h}(i)\left(\frac{2a-2b}{a}\right) + \Psi^{n-1}_{e,h}(i)(-1) + \Psi^{n}_{e,h}(i-1)\left(\frac{b}{a}\right) \tag{6}$$

and in the nodes between dielectric interfaces of step discontinuities (inhomogeneous region) becomes:

$$\Psi^{n+1}_{e,h}(i) = \Psi^{n}_{e,h}(i+1)\left(\frac{b}{a'}\right) + \Psi^{n}_{e,h}(i)\left(\frac{2a'-2b}{a'}\right) + \Psi^{n-1}_{e,h}(i)(-1) + \Psi^{n}_{e,h}(i-1)\left(\frac{b}{a'}\right) \tag{7}$$

with [4]

$$\begin{aligned} a &= \frac{\mu\varepsilon}{(\Delta t)^2} \\ a' &= a + \frac{\mu\Delta\varepsilon}{(\Delta t)^2} \\ b &= \frac{1}{(\Delta z)^2} \end{aligned} \tag{8}$$

We observe that the Eq. (3) gives convergent solutions by considering also a non fine spatial discretisation, by decreasing the computational cost [5]. In a nonlinear material the wave equation Eq. (1) becomes

$$\nabla^2\Psi_{\mathrm{e,h}}(\mathrm{x,y,z,t}) - \mu_0\varepsilon_0 n^2 \frac{\partial^2\Psi_{\mathrm{e,h}}(\mathrm{x,y,z,t})}{\partial t^2} - \mu_0\varepsilon_0 \frac{\partial^2 P^{e,h}{}_{NL}(\mathrm{x,y,z,t})}{\partial t^2} = 0 \tag{9}$$

where $P^{e,h}{}_{NL}$ is the polarization given by $P^{e,h}{}_{NL} = \chi^{(2)}\Psi_{\mathrm{e}}\Psi_{\mathrm{h}}$, n is the material refractive index, and $\chi^{(2)}$ is the dispersionless nonlinear susceptibility. The general field formulation considers three different fields propagating at three different frequencies $\Psi_{\mathrm{e}}(\omega_1)$, $\Psi_{\mathrm{h}}(\omega_2)$, $\Psi_{\mathrm{g}}(\omega_3)$ in material exhibiting an instantaneous second-order nonlinearity

$$\nabla^2\Psi_{\mathrm{e}} = \mu_0\varepsilon_0 n_a{}^2 \frac{\partial^2\Psi_{\mathrm{e}}}{\partial t^2} + \mu_0\varepsilon_0\chi^{(2)}(\omega_1)\frac{\partial^2(\Psi_{\mathrm{h}}\Psi_g)}{\partial t^2} \tag{10}$$

$$\nabla^2\Psi_{\mathrm{h}} = \mu_0\varepsilon_0 n_b{}^2 \frac{\partial^2\Psi_{\mathrm{h}}}{\partial t^2} + \mu_0\varepsilon_0\chi^{(2)}(\omega_2)\frac{\partial^2(\Psi_{\mathrm{e}}\Psi_g)}{\partial t^2} \tag{11}$$

#97297 - $15.00 USD Received 10 Jun 2008; revised 22 Jul 2008; accepted 1 Aug 2008; published 2 Sep 2008

$$\nabla^2\Psi_g = \mu_0\varepsilon_0 n_c^{\,2}\frac{\partial^2\Psi_g}{\partial t^2} + \mu_0\varepsilon_0\chi^{(2)}(\omega_3)\frac{\partial^2(\Psi_e\Psi_h)}{\partial t^2} \tag{12}$$

where n_a, n_b, n_c are the refractive indexes of the wave $\Psi_e(\omega_1)$, $\Psi_h(\omega_2)$, $\Psi_g(\omega_3)$ respectively. We observe that in a generic case $\chi^{(2)}$ is a tensor and Eq. (10), Eq. (11) and Eq. (12) becomes systems of scalar equations to be solved for each crystal-direction. However most semiconductor, which crystallize in zinc-blende structures, have a symmetry and their second-order susceptibility has a single nonzero independent component (for GaAs at the transparency region below the optical energy gap $\chi_{x,y,z}^{(2)}$= 200 pm/V).

Coupled equations Eq. (10), Eq. (11), and Eq. (12) can be rewritten as

$$\nabla^2\Psi_e = \mu_0\varepsilon_0 n_a^{\,2}\frac{\partial^2\Psi_e}{\partial t^2} + \mu_0\varepsilon_0\chi^{(2)}(\omega_1)\cdot \cdot\left(\Psi_h\frac{\partial^2\Psi_g}{\partial t^2} + \Psi'_h\frac{\partial^2\Psi_h}{\partial t^2} + 2\frac{\partial\Psi_h}{\partial t}\frac{\partial\Psi_g}{\partial t}\right) \tag{13}$$

$$\nabla^2\Psi_h = \mu_0\varepsilon_0 n_b^{\,2}\frac{\partial^2\Psi_h}{\partial t^2} + \mu_0\varepsilon_0\chi^{(2)}(\omega_2)\cdot \cdot\left(\Psi_e\frac{\partial^2\Psi_g}{\partial t^2} + \Psi'_h\frac{\partial^2\Psi_e}{\partial t^2} + 2\frac{\partial\Psi_e}{\partial t}\frac{\partial\Psi_g}{\partial t}\right) \tag{14}$$

$$\nabla^2\Psi_g = \mu_0\varepsilon_0 n_c^{\,2}\frac{\partial^2\Psi_g}{\partial t^2} + \mu_0\varepsilon_0\chi^{(2)}(\omega_3)\cdot \cdot\left(\Psi_e\frac{\partial^2\Psi_h}{\partial t^2} + \Psi_h\frac{\partial^2\Psi_e}{\partial t^2} + 2\frac{\partial\Psi_e}{\partial t}\frac{\partial\Psi_h}{\partial t}\right) \tag{15}$$

We observe that Eq. (13), Eq. (14) and Eq. (15) for a generic three-wave-mixing process can refer also to a twin photon generation process [9].

The fundamental and the second harmonic field in a SHG process, occurs whit $\omega_1=\omega_2=\omega$, $\omega_3=\omega_1+\omega_2=2\omega$, $\chi^{(2)}=\chi^{(2)}(\omega_1)/2=\chi^{(2)}(\omega_3)$ [3], and $\Psi^f = \Psi_e = \Psi_h$ ($n_a = n_b = n_f$), and $\Psi^s = \Psi_g$ ($n_c = n_s$). In this case the coupled equations to solve are the following

$$\nabla^2\Psi^f = \mu_0\varepsilon_0 n_f^{\,2}\frac{\partial^2\Psi^f}{\partial t^2} + 2\mu_0\varepsilon_0\chi^{(2)}\cdot \cdot\left(\Psi^f\frac{\partial^2\Psi^s}{\partial t^2} + \Psi^s\frac{\partial^2\Psi^f}{\partial t^2} + 2\frac{\partial\Psi^f}{\partial t}\frac{\partial\Psi^s}{\partial t}\right) \tag{16}$$

$$\nabla^2\Psi^s = \mu_0\varepsilon_0 n_s^{\,2}\frac{\partial^2\Psi^s}{\partial t^2} + 2\mu_0\varepsilon_0\chi^{(2)}\cdot \cdot\left(\Psi^f\frac{\partial^2\Psi^f}{\partial t^2} + \frac{\partial\Psi^f}{\partial t}\frac{\partial\Psi^f}{\partial t}\right) \tag{17}$$

We observe from Eq. (16) and Eq. (17) that the fundamental Ψ^f and the second harmonic Ψ^s field are characterized by the refractive indexes n_f and n_s respectively. For the asymmetrical slab shown in Fig. 1 (a), n_f represents the effective refractive index along the x-direction at $\omega_1=\omega_s$ and n_s represents the effective refractive index at $\omega_3=\omega_f=2\omega_s$. In this way it is possible to model the SHG by two transmission lines as reported in Fig. 1 (b), each one characterized by the characteristic impedance of Eq. (2), as

#97297 - $15.00 USD Received 10 Jun 2008; revised 22 Jul 2008; accepted 1 Aug 2008; published 2 Sep 2008

$$Z_f = \frac{1}{n_f}\sqrt{\frac{\mu_0}{\varepsilon_0}} \ , \ Z_s = \frac{1}{n_s}\sqrt{\frac{\mu_0}{\varepsilon_0}} \tag{18}$$

By using the finite difference (FD) discretisation Eq. (16) and Eq. (17) become

$$\begin{aligned}&\frac{\Psi_f^n(i+1)-2\Psi_f^n(i)+\Psi_f^n(i-1)}{\Delta^2 z}=\mu_0\varepsilon_0 {n_f}^2\frac{\Psi_f^{n+1}(i)-2\Psi_f^n(i)+\Psi_f^{n-1}(i)}{\Delta^2 t}+2\mu_0\varepsilon_0\chi^{(2)}\cdot\\&\cdot\left(\Psi_f^n(i)\frac{\Psi_s^{n+1}(i)-2\Psi_s^n(i)+\Psi_s^{n-1}(i)}{\Delta^2 t}+\Psi_s^n(i)\frac{\Psi_f^{n+1}(i)-2\Psi_f^n(i)+\Psi_f^{n-1}(i)}{\Delta^2 t}+\right.\\&\left.+2\cdot\frac{\Psi_f^{n+1/2}(i)-\Psi_f^{n-1/2}(i)}{\Delta t}\cdot\frac{\Psi_s^{n+1/2}(i)-\Psi_s^{n-1/2}(i)}{\Delta t}\right)\end{aligned} \tag{19}$$

$$\begin{aligned}&\frac{\Psi_s^n(i+1)-2\Psi_s^n(i)+\Psi_s^n(i-1)}{\Delta^2 z}=\mu_0\varepsilon_0 {n_s}^2\frac{\Psi_s^{n+1}(i)-2\Psi_s^n(i)+\Psi_s^{n-1}(i)}{\Delta^2 t}+2\mu_0\varepsilon_0\chi^{(2)}\cdot\\&\cdot\left(\Psi_f^n(i)\frac{\Psi_f^{n+1}(i)-2\Psi_f^n(i)+\Psi_f^{n-1}(i)}{\Delta^2 t}+\frac{\Psi_f^{n+1/2}(i)-\Psi_f^{n-1/2}(i)}{\Delta t}\cdot\frac{\Psi_f^{n+1/2}(i)-\Psi_f^{n-1/2}(i)}{\Delta t}\right)\end{aligned} \tag{20}$$

where *i* represents the cell position in the z-propagation direction and *n* represent the time step. By separating the $\Psi^{n+1}{}_f(i)$ in eq. (19) and $\Psi^{n+1}{}_s(i)$ in Eq. (20) we obtain the iterative form of the fundamental and the second harmonic field as

$$\begin{aligned}&\Psi_f^{n+1}(i)\cdot(\mu_0\varepsilon_0 {n_f}^2\Delta^2 z+2\mu_0\varepsilon_0\chi^{(2)}\Delta^2 z\Psi_s^n(i))=\Psi_f^n(i)\cdot[(-2\Delta^2 t+2\mu_0\varepsilon_0 {n_f}^2\Delta^2 z-\\&-2\mu_0\varepsilon_0\chi^{(2)}\Delta^2 z\cdot(\Psi_s^{n+1}(i)-2\Psi_s^n(i)+\Psi_s^{n-1}(i))-2\mu_0\varepsilon_0\chi^{(2)}\Delta^2 z\Psi_s^n(i)]+\\&+4\mu_0\varepsilon_0\chi^{(2)}\Delta^2 z\Psi_f^{n+1/2}(i)\cdot(-\Psi_s^{n+1/2}(i)+\Psi_s^{n-1/2}(i))+\\&+4\mu_0\varepsilon_0\chi^{(2)}\Delta^2 z\Psi_f^{n-1/2}(i)\cdot(\Psi_s^{n+1/2}(i)-\Psi_s^{n-1/2}(i)))\end{aligned} \tag{21}$$

$$\begin{aligned}&\Psi_s^{n+1}(i)\cdot(\mu_0\varepsilon_0 {n_s}^2\Delta^2 z)=\Psi_s^n(i+1)\Delta^2 t+\Psi_s^n(i)(2\mu_0\varepsilon_0 {n_s}^2\Delta^2 z-2\Delta^2 t)+\\&+\Psi_s^n(i-1)\Delta^2 t-\Psi_s^{n-1}(i)\mu_0\varepsilon_0 {n_s}^2\Delta^2 z-\Psi_f^n(i)\Psi_f^{n+1}(i)2\mu_0\varepsilon_0\chi^{(2)}\Delta^2 z+\\&+\Psi_f^n(i)\Psi_f^n(i)4\mu_0\varepsilon_0\chi^{(2)}\Delta^2 z-\Psi_f^n(i)\Psi_f^{n-1}(i)2\mu_0\varepsilon_0\chi^{(2)}\Delta^2 z-\\&-\Psi_f^{n+1/2}(i)\Psi_f^{n+1/2}(i)2\mu_0\varepsilon_0\chi^{(2)}\Delta^2 z+\Psi_f^{n+1/2}(i)\Psi_f^{n-1/2}(i)2\mu_0\varepsilon_0\chi^{(2)}\Delta^2 z+\\&+\Psi_f^{n-1/2}(i)\Psi_f^{n+1/2}(i)2\mu_0\varepsilon_0\chi^{(2)}\Delta^2 z-\Psi_f^{n-1/2}(i)\Psi_f^{n-1/2}(i)2\mu_0\varepsilon_0\chi^{(2)}\Delta^2 z\end{aligned} \tag{22}$$

The absorbing boundary conditions (ABCs) [10],[11] around the computational domain Ω, permit all outward-propagating numerical waves to exit Ω, as if the simulations were performed on a computational domain of infinite extent. In this case, extremely small boundary reflection coefficient of the order of 10^{-11} is obtained in the simulations by enhancing the accuracy of the solution allowing for long simulation times steps.

3. QPM condition and time domain results: SH generation in GaAs discontinuous waveguide.

Usually high intensity sources are necessary in order to observe a SH in a $\chi^{(2)}$ nonlinear structure. For this purpose a nonlinear waveguide with dielectric step discontinuities can increase the SH efficiency conversion. The proper choice of the grating periodicity can increase the SH intensity: the grating is designed to restore the proper phase relationship between the fundamental wave and the second harmonic in the presence of dispersion, thereby improving the efficiency of second-harmonic generation. The QPM technique is a practical method of substantially increasing the second-harmonic power by effectively reducing the phase mismatch between the fundamental and the SH fields: the technique relies on

#97297 - $15.00 USD Received 10 Jun 2008; revised 22 Jul 2008; accepted 1 Aug 2008; published 2 Sep 2008

introducing a grating in the waveguide to compensate for the difference of the propagation refractive indexes in the waveguide $\Delta n = n_s - n_f$. It is useful to define the coherence length [12], [13]:

$$Lc = \frac{\pi}{|2\beta_f - \beta_{SH}|} = \frac{\lambda_0^f}{4|n_f - n_s|} \tag{23}$$

where β_f and β_{SH} are the propagation constant of the fundamental and the SH, respectively; λ_0^f is the free-space wavelength of the fundamental wave; and n_f and n_s are the effective indices at the fundamental and second-harmonic frequencies, respectively. *Lc* represents the length scale when the fundamental and harmonic get out of phase by π radians with a corresponding mismatch in wave-*k* vectors of $\Delta k = k^{SH} - 2k^f = 2k_0 \Delta n$ [12], where $k_0 = 2\pi/\lambda_0^f$, k^{SH} and k^f are the waves vectors for the SH and fundamental waves, respectively. The QPM condition, applied to the grating period, is given by the relationship:

$$\frac{2\pi}{\Lambda} = \Delta k \tag{24}$$

which is equivalent to $\Lambda = 2L_C$.

In order to test the accuracy of the time domain method presented in this work we compare the published experimental results [13] of a QPM GaAS structure. By considering the QPM technique we model a QPM semiconductor [13] device based on a methodology that involves a periodically switched nonlinearity. In this case a periodic modulation of the susceptibility coefficient along the direction of light-beam propagation is considered. As first implementation of Eq. (21) and Eq. (22) we model a grating periodicity given by $\chi_{GaAs}^{(2)} > \chi_{Al_xGa_{1-x}As}^{(2)}$ (see inset of Fig. 3). The coupled Eq. (21) and Eq. (22) with the circuital approach given by Eq. (6) and Eq. (7) and the EDC method, provide a good agreement with experimental SH intensity results of [13]: Fig. 3 shows the accuracy and the convergence of the numerical coupled equations. Figure 3 shows the ratio between the output SH power and the fundamental output power with respect to the input power. In particular the left vertical axis shows the numerical results, whereas on the vertical right axis is reported the experimental behavior (see [13]). Another verification of the time domain model is given by the frequency response reported in Fig. 4 (a) and (b) in which we show the SH and the fundamental simulated spectra obtained through the discrete Fourier transform (DFT) of the signals (evaluated at the end of the simulated waveguide) related to the fundamental signal (λ_0^f =1.955 μm) and to the SH signal (λ_0^s =0.9775 μm), respectively. A good agreement with the experimental spectra of [13] is observed.

After this validation we calculate numerically the SH efficiency of a GaAs waveguide with a working wavelength λ_0^f =1.55 μm (SH at λ_0^s =0.775 μm). In this case the simulated structure is characterized by a QPM grating with Λ=6.021μm ($L_c = L_s = \Lambda/2$), $\chi^{(2)}$ (GaAs)=200 pm/V, n_1(GaAs at λ_0^f =1.55 μm)=3.374, n_2=3. In Fig. 5 is shown the time domain evolution of the fundamental and of the SH field by exciting the periodic structure with a sinusoidal signal at λ_0^f =1.55 μm: the coupled Eq. (21) and Eq. (22) generate automatically the SH coupled field which propagates in the asymmetrical slab waveguide. For the same structure, Fig. 6 shows the fundamental and the SH spectrum, by considering, as source, a carrier modulated by an exponential signal defined by (see time evolution in Fig. 6 (a)):

$$\Psi_f = \exp(-(t \cdot \Delta t / T_0)^2) \cdot \cos(\omega^f{}_0 \cdot t \cdot \Delta t) \tag{25}$$

#97297 - $15.00 USD Received 10 Jun 2008; revised 22 Jul 2008; accepted 1 Aug 2008; published 2 Sep 2008

where ω_0^f is the fundamental angular frequency, Δt is the time steps and the constant T_0 represents the modulation of the fundamental carrier.

We observe from Fig. 6 (b) that the shape of the DFT signal spectrum may change with the parameter T_0 defined in the source signals shown in Fig. 6 (a). The effect of the grating efficiency on the SH generation is observed in Fig. 7 in which is reported the SH amplitude in the case of uniform waveguide (without grating), and in the case of QPM waveguide (with grating): an increase of SH amplitude of two order of magnitude is observed, confirming the efficiency of the QPM grating in the enhancement of the SH signal.

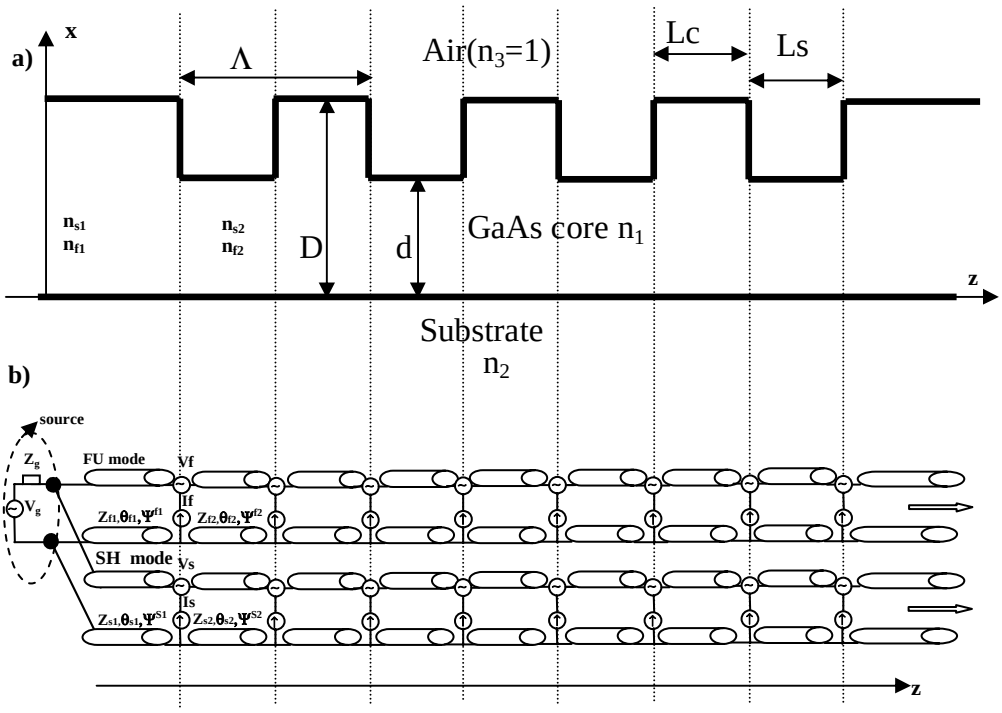

Fig. 1. (a) Asymmetrical slab waveguide with nonlinear GaAs core, n_{s1} and n_{f1} are the effective refractive indexes (SH index and fundamental index respectively) of the region characterized by the thickness D, n_{s2} and n_{f2} are the effective refractive indexes (SH index and fundamental index respectively) of the region characterized by the thickness d; (b) and related transmission line model with generators at discontinuous interfaces.

#97297 - $15.00 USD Received 10 Jun 2008; revised 22 Jul 2008; accepted 1 Aug 2008; published 2 Sep 2008

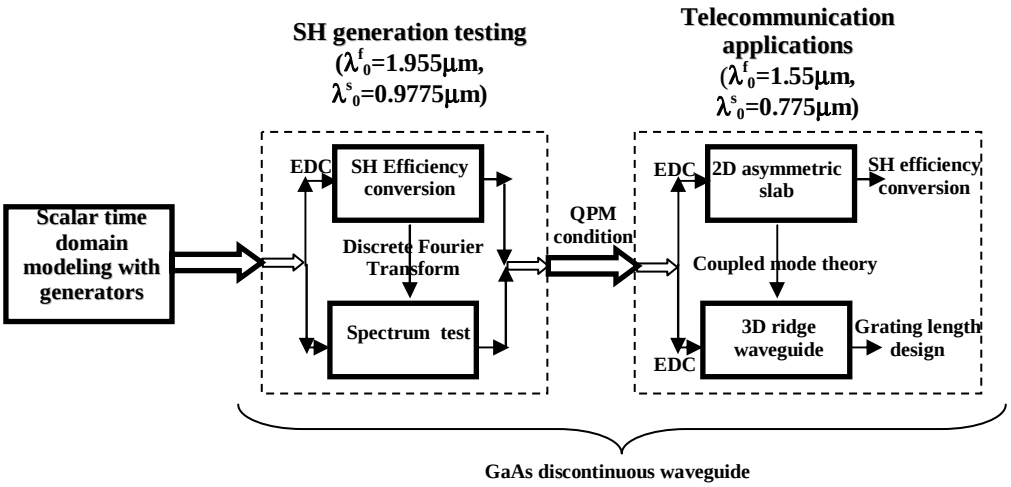

Fig. 2. Block diagram: analysis of SH generation process in discontinuous GaAs waveguide. The testing is related to experimental results of [13].

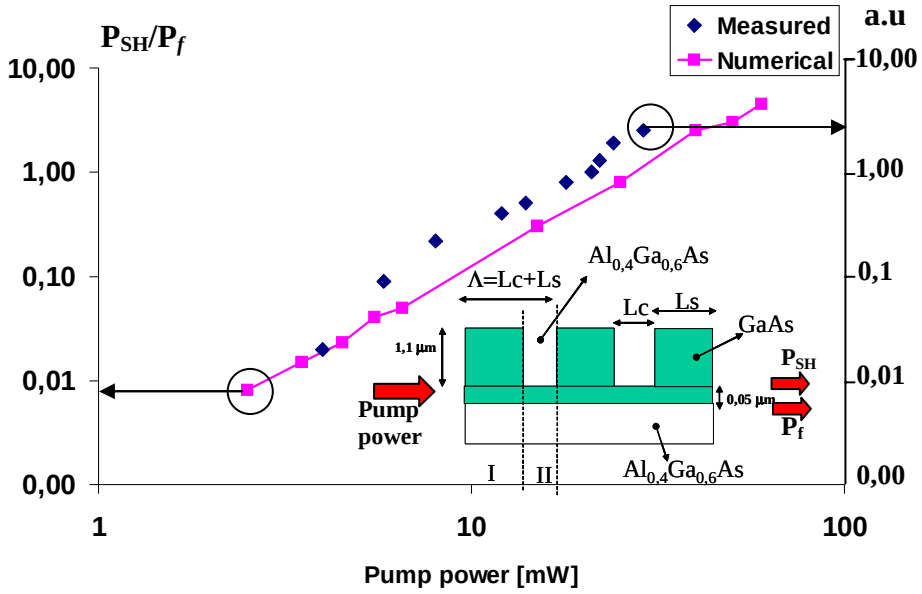

Fig. 3. Measured and scalar time domain numerical results of a periodic GaAs/$Al_{0,4}Ga_{0,6}As$ waveguide. Inset: simulated structure with *Lc*=2.97 μm, *Ls*=4.73 μm. The effective indexes of the region I are: n_{s1}= 3.321, n_{f1}= 3.29; the effective indexes of the region II are n_{s2}= 3.1651, n_{f2}= 3.161. The time step used in the simulation is $\Delta t=1.6679*10^{-16}$ sec. and the spatial step is $\Delta z=5*10^{-8}$ m. P_{SH} refers to the SH output power.

#97297 - $15.00 USD Received 10 Jun 2008; revised 22 Jul 2008; accepted 1 Aug 2008; published 2 Sep 2008

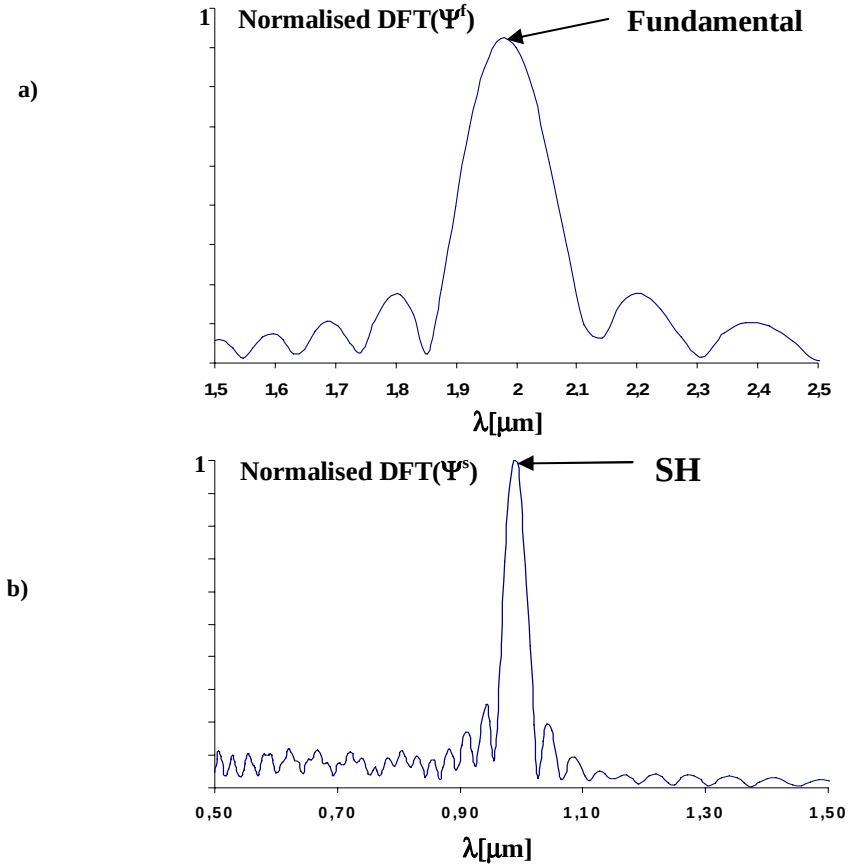

Fig. 4. Normalized discrete Fourier transform DFT at the end of the simulated waveguide of: a) fundamental mode Ψ^f, and b) SH mode Ψ^s, respectively.

#97297 - $15.00 USD Received 10 Jun 2008; revised 22 Jul 2008; accepted 1 Aug 2008; published 2 Sep 2008

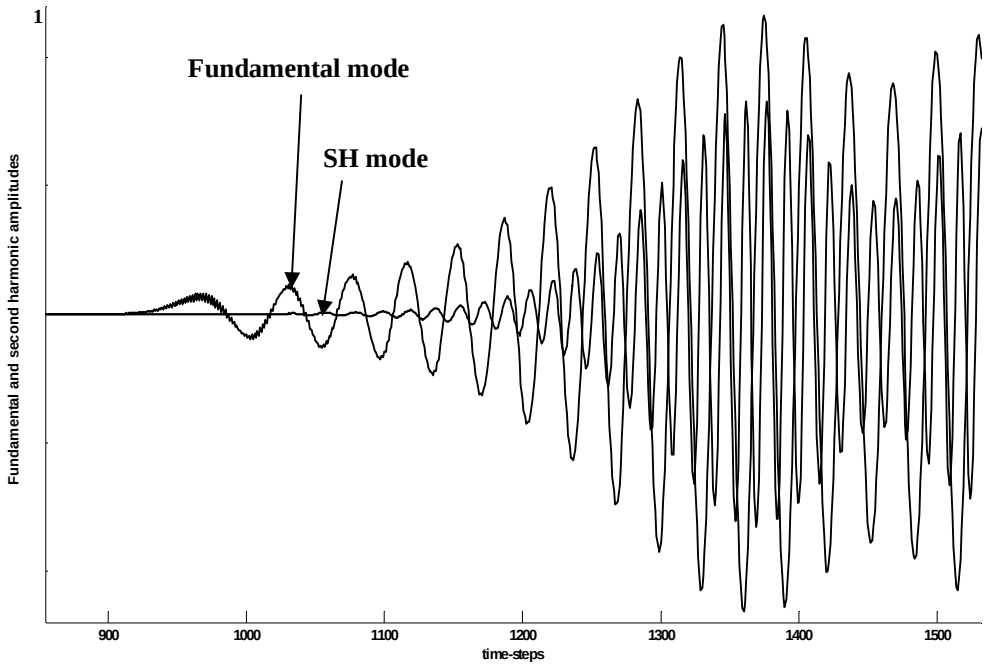

Fig. 5. Time evolution of the normalized fundamental (λ_0^f=1.55 μm) and SH (λ_0^S=0.775 μm) signals generated at the end of grating region in an asymmetrical slab waveguide with nonlinear GaAs core: $\chi^{(2)}$=200 pm/V, d=0.22 μm, D=0.36 μm, Λ= 6.021 μm (QPM condition), n_{s1}=3.2313, n_{f1}=3.1052, n_{s2}=3.3187, n_{f2}=3.1895. The total grating length is 5Λ.

#97297 - $15.00 USD Received 10 Jun 2008; revised 22 Jul 2008; accepted 1 Aug 2008; published 2 Sep 2008

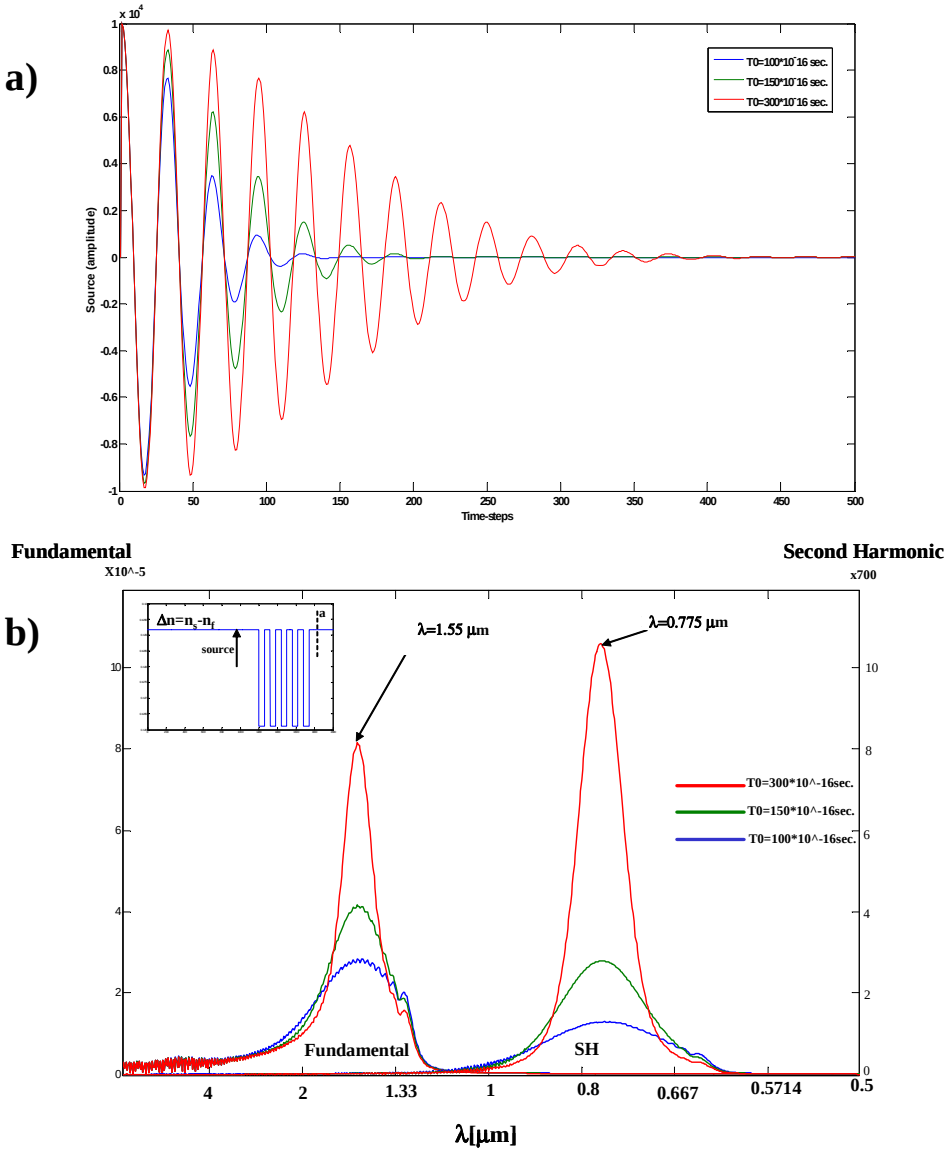

Fig. 6. (a) Pump source signals for different T_0 values. (b) Fundamental and SH spectrum for different T_0 values at the end of the grating (section *a* of the inset). The time step used in the simulation is $\Delta t=1.6679*10^{-16}$ sec. and the spatial step is $\Delta z=5*10^{-8}$ m.

#97297 - $15.00 USD Received 10 Jun 2008; revised 22 Jul 2008; accepted 1 Aug 2008; published 2 Sep 2008

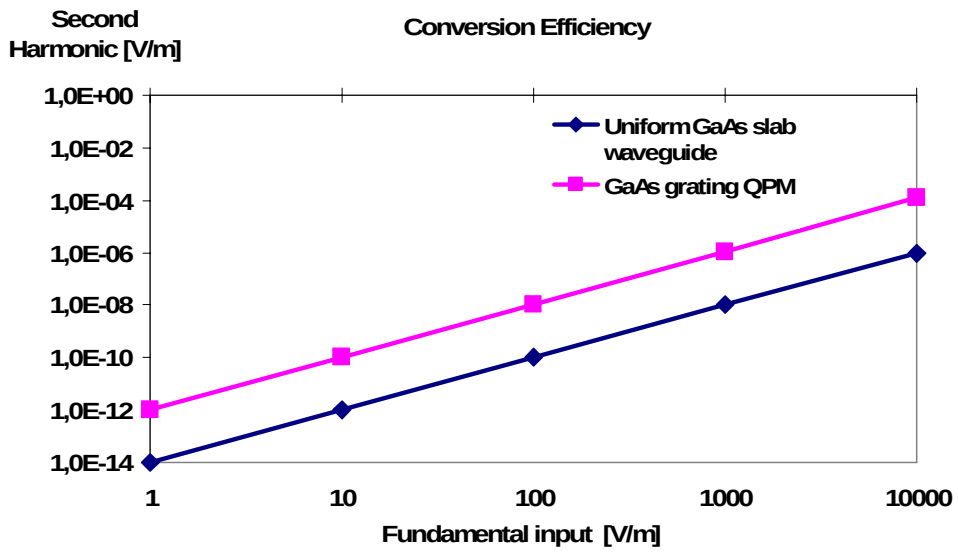

Fig. 7. SH conversion efficiency in the case of uniform GaAs slab waveguide and of QPM GaAs grating and sinusoidal source as pump signal.

4. SH process coupling in GaAs ridge waveguide and grating length design.

The analytical approach of the coupling mode theory provides an alternative design criterium of grating length: the length of the step discontinuities (total grating length) can be chosen in order to obtain at the end of the grating a maximum SH signal corresponding to a maximum coupling coefficient. As application of this analytical model we analyze a typical optical 3D periodic waveguide commonly used in multiplexing or filtering applications, such as ridge waveguide shown in Fig. 8 (a) characterized by GaAs core on $Al_{0,7}Ga_{0,3}As$ substrate at working wavelength of λ_0=1.55 μm.

This 3D waveguide can be analyzed in 2D dimension by the EDC [14] method, and the coupling mode theory provides the longitudinal position in which the coupling between the fundamental mode and the generated SH mode is characterized by an high intensity. For this structure we find through the time-domain modeling the same order of the conversion efficiency reported in Fig. 7. With the help of the analytical coupled theory approach it is also possible to define the minimum grating length for the best power conversion. In the EDC approach [14] we separately analyze region I and region II shown in Fig. 8 (b): we first evaluate the propagation constants in the y-directions then the effective constants ε_I ,and ε_{II} (belonging to region I and II); finally we evaluate the propagation constant in the x-direction. The coupling coefficient $C_{f,S}$ couples the fundamental mode A^f and the SH mode B^S, as reported by the following linear simplified coupled-mode equations [15],[16]:

$$\begin{aligned} \frac{dA^f(z)}{dz} &= -jC_{f,S}(z)B^S(z)A^f(z)^* \exp(-j2\delta z) \\ \frac{dB^S(z)}{dz} &= -jC_{S,f}(z)[A^f(z)]^2 \exp(-j2\delta z) \end{aligned} \tag{26}$$

#97297 - $15.00 USD Received 10 Jun 2008; revised 22 Jul 2008; accepted 1 Aug 2008; published 2 Sep 2008

where $2\delta=\beta_{SH} - (2\beta_f + \Delta k)$. The coupling coefficient $C_{f,S}(z)$ is obtained by the coupling mode theory [13]

$$C_{f,S}(z) = \omega_0^f \int_{-\infty}^{+\infty}\int_{-\infty}^{+\infty} \Delta\varepsilon(z) E^t{}_f E^t{}_S dxdy \tag{27}$$

where E^t_f and E^t_S are the fundamental and the SH transverse field components associated to the lowest order modes of fundamental and SH waves respectively, and $\Delta\varepsilon(z)$ represents the variation of the refractive index along the longitudinal z-direction. This variation $\Delta\varepsilon(z)$ is a square-wave given by the Fourier series:

$$\Delta\varepsilon(z) = \frac{1}{\pi}\sum_{l=1}^{\infty}\left(\frac{n_1^2 - n_3^2}{l}\right)\cdot\sin\left(\frac{2l\pi z}{L_c + L_s}\right) \tag{28}$$

We observe that Eq. (26) refers to a periodic structure with linear material. This ideal assumption is used in order to estimate the grating length related to a good coupling condition between the fundamental and SH guided modes not considering the losses. In Fig. 9 are shown the coupling coefficients $C_{f,S}(z)$ in QPM condition and for different lengths (no phase matching condition) L_c and L_s: in the no phase matching cases the coupling coefficients will show other minima which decrease the efficiency conversion.

The analyzed ridge waveguide is characterized by a single transverse electric TE mode [14] obtained with a working wavelength of λ_0^f =1.55 μm (E^t_f profile of the single TE propagating mode), and with a working wavelength of λ_0^s =0.775 μm (E^t_S profile of the single TE propagating mode). The fixed parameters chosen in the evaluation of the coupling coefficient are: n_1(GaAs)=3.374, n_3(air)=1, n_2($Al_{0.7}Ga_{0.3}As$)=3.02, s=0.4 μm, d=0.2 μm, D= 0.32 μm. In Fig. 10 are shown the power associated to the fundamental field ($|A^f(z)|^2$), and the power ($|B^S(z)|^2$) associated to the SH field: $A^f(z)$ and $B^S(z)$ are solutions of Eq. (26) in the case of QPM condition. Figure 11 shows the peak development of the SH mode and the dip development of the fundamental one reported in Fig. 10. It is clear from both the figures how the best coupling condition is found around z=1.25 μm (minimum grating length) where the coupling coefficient between the two modes and the SH power are maximum, and the fundamental power is minimum.

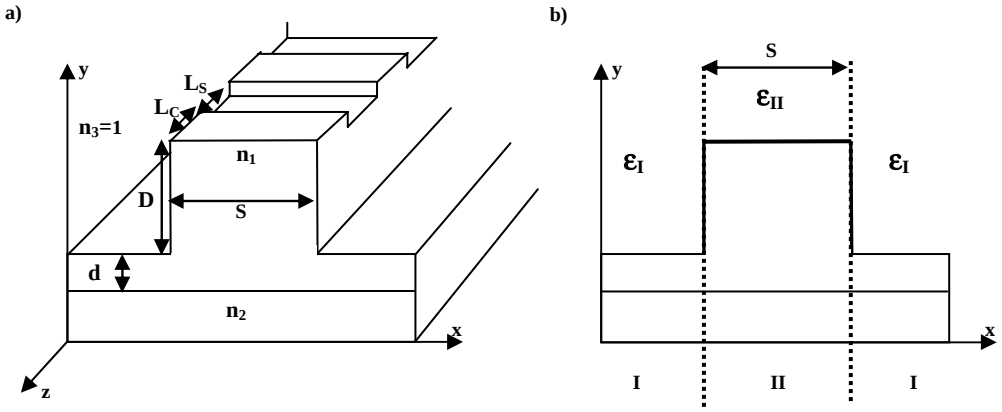

Fig. 8. (a) 3D ridge waveguide with nonlinear GaAs core; (b) EDC approach.

#97297 - $15.00 USD Received 10 Jun 2008; revised 22 Jul 2008; accepted 1 Aug 2008; published 2 Sep 2008

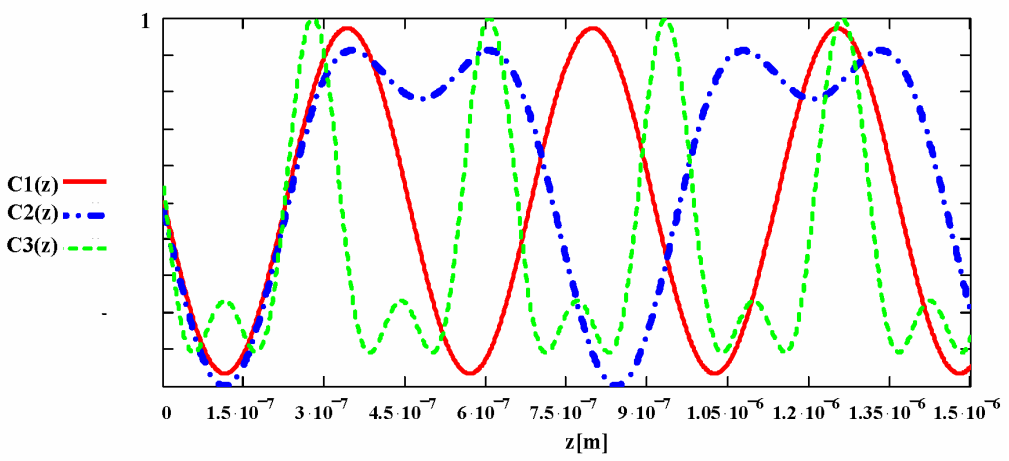

Fig. 9. Coupling coefficients $C_{f,S}(z)$ for different values of L_c and L_S . $C_{f,S}(z)$ =C1(z) refers to a QPM grating with L_C=L_S=0.2275μm, $C_{f,S}(z)$ =C2(z) refers to a grating with L_C=0.2275μm and L_S=0.5 μm, and finally $C_{f,S}(z)$ =C3(z) refers to a grating with L_C=0.2275μm and L_S=0.1 μm.

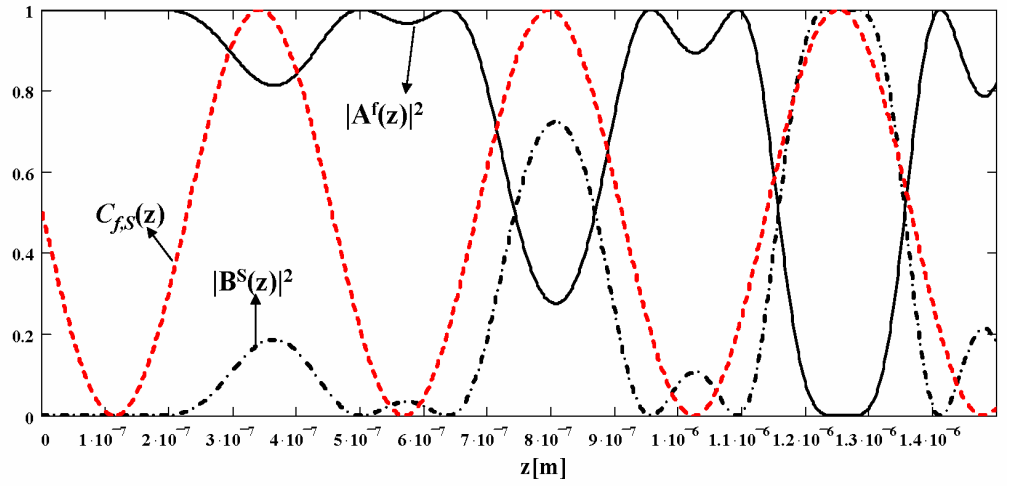

Fig. 10. Ridge waveguide (QPM condition): $|A^f(z)|^2$,$|B^S(z)|^2$, and $C_{f,S}(z)$ are the fundamental, the SH and the coupling coefficient amplitudes, respectively. The initial value $|A^f(z=0)|^2$=1 represents the pump signal.

#97297 - $15.00 USD Received 10 Jun 2008; revised 22 Jul 2008; accepted 1 Aug 2008; published 2 Sep 2008

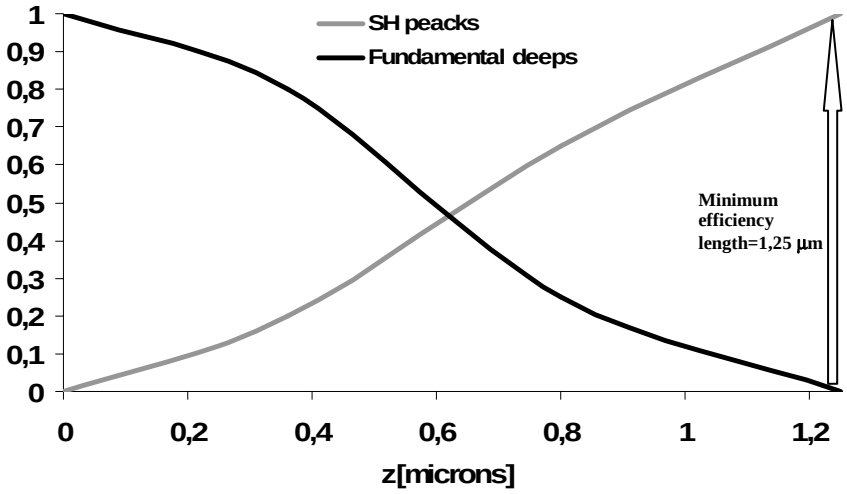

Fig. 11. SH mode peak development and fundamental mode dip development. The minimum length of coupling efficiency is at z=1,25 μm. The coupling efficiency is obtained with the ideal assumption of no mode-losses.

5. Conclusion

A flexible and computationally efficient circuital approach regarding to the second-order nonlinear processes is presented. The scalar potential modeling is applied to nonlinear GaAs optical waveguide with step discontinuities by providing a good agreement with the published experimental results. With the help of the EDC method, the scalar potential method can be generalized to complex 3D optical waveguides such as nonlinear ridge waveguides. The rigorous analysis of the fundamental/SH coupled equations provides the conversion efficiency of the GaAs/QPM grating. The circuital approach can be extended to twin photon generation process through the three wave mixing coupled wave equations.

#97297 - $15.00 USD Received 10 Jun 2008; revised 22 Jul 2008; accepted 1 Aug 2008; published 2 Sep 2008